Ultrasound in Med. & Biol., Vol. 39, No. 11, pp. 1983–1990, 2013

0301-5629/$ - see front matter

http://dx.doi.org/10.1016/j.ultrasmedbio.2013.03.025

● *Original Contribution*

ULTRASOUND-MEDIATED MICROBUBBLE ENHANCEMENT OF RADIATION THERAPY STUDIED USING THREE-DIMENSIONAL HIGH-FREQUENCY POWER DOPPLER ULTRASOUND

Sheldon J. J. Kwok,*†‡§ Ahmed El Kaffas,*†‡§ Priscilla Lai,‡§ Azza Al Mahrouki,*‡ Justin Lee,*†‡§ Sara Iradji,‡§ William Tyler Tran,‡§ Anoja Giles,*‡ and Gregory J. Czarnota*†‡§

*Radiation Oncology, Sunnybrook Health Sciences Centre, Toronto, Ontario, Canada; †Department of Radiation Oncology, University of Toronto, Toronto, Ontario, Canada; ‡Imaging Research, Sunnybrook Health Sciences Centre, Toronto, Ontario, Canada; and §Department of Medical Biophysics, University of Toronto, Toronto, Ontario, Canada

(*Received* 20 *June* 2012; *revised* 18 *March* 2013; *in final form* 23 *March* 2013)

Abstract—Tumor responses to high-dose (>8 Gy) radiation therapy are tightly connected to endothelial cell death. In the study described here, we investigated whether ultrasound-activated microbubbles can locally enhance tumor response to radiation treatments of 2 and 8 Gy by mechanically perturbing the endothelial lining of tumors. We evaluated vascular changes resulting from combined microbubble and radiation treatments using high-frequency 3-D power Doppler ultrasound in a breast cancer xenograft model. We compared treatment effects and monitored vasculature damage 3 hours, 24 hours and 7 days after treatment delivery. Mice treated with 2 Gy radiation and ultrasound-activated microbubbles exhibited a decrease in vascular index to 48 ± 10% at 24 hours, whereas vascular indices of mice treated with 2 Gy radiation alone or microbubbles alone were relatively unchanged at 95 ± 14% and 78 ± 14%, respectively. These results suggest that ultrasound-activated microbubbles enhance the effects of 2 Gy radiation through a synergistic mechanism, resulting in alterations of tumor blood flow. This novel therapy may potentiate lower radiation doses to preferentially target endothelial cells, thus reducing effects on neighboring normal tissue and increasing the efficacy of cancer treatments. (E-mail: Gregory.Czarnota@sunnybrook.ca) **Crown Copyright © 2013 Published by Elsevier Inc. on behalf of World Federation for Ultrasound in Medicine & Biology.**

Key Words: **Ultrasound-activated microbubbles, Microbubble perturbation, Radiation therapy, Power Doppler ultrasound, Tumor vasculature, Vascular disrupting agents, High-frequency ultrasound, Tumor vascular imaging, Radiotherapy.**

INTRODUCTION

Radiation therapy is an important and widely used cancer treatment. It has been shown to act, on the molecular level, by inducing biochemical lesions in the DNA of cancer cells, leading to tumor cell death (Lehnert 2007). Recent articles have reported that radiation can also act by directly damaging tumor vasculature, leading to secondary tumor cell death (El Kaffas et al. 2012; Folkman and Camphausen 2001; Fuks and Kolesnick 2005; Garcia-Barros et al. 2003; Paris et al. 2001). These observations were made after single large doses of radiation (>8 Gy) were delivered to the tumor, leading to rapid endothelial cell apoptosis through an acid sphingomyelinase-dependent pathway. Taken together, these findings suggest that endothelial cells may be important regulators of tumor response to therapy. Agents capable of enhancing the response of tumor endothelial cells would potentially improve tumor responses to radiation therapy, while lowering the total dose of ionizing radiation needed for tumor cure.

We describe here a novel approach to mechanical perturbation of the endothelial lining of tumor vasculature using ultrasound-activated microbubbles. The aim of this study was to enhance direct endothelial cell apoptosis and secondary overall tumor response to radiation. Microbubbles are micron-sized spheres of gas, usually a perfluorocarbon, stabilized within a thin shell of biocompatible material, such as a protein or lipid. They are administered through peripheral venous injection and can pass through the systemic circulation. These

Address correspondence to: Gregory J. Czarnota, Department of Radiation Oncology, Sunnybrook Health Sciences Centre, 2075 Bayview Avenue, T2–067, Toronto, ON M4 N 3 M5, Canada. E-mail: Gregory.Czarnota@sunnybrook.ca

microbubbles are already used extensively as contrast agents for ultrasound (Wilson and Burns 2006). When activated with specific ultrasound frequencies, microbubbles exhibit resonant behaviors, oscillate non-linearly and eventually rupture when sufficient ultrasound energy is applied (Qin and Ferrara 2007). These properties make microbubbles suitable for a number of therapeutic uses, including dissolution of blood clots, activation and delivery of drugs and opening of the blood–brain barrier (Unger et al. 2002, 2004). Ultrasound-stimulated microbubbles can perturb the function of surrounding cells, destroy local vasculature or enhance vascular permeability (Hwang et al. 2005; Wu and Nyborg 2008). In this study, we found that low-mechanical-index ultrasound-mediated activation of microbubbles can enhance the effects of radiation in a breast cancer xenograft model.

To evaluate tumor vascular changes resulting from combined ultrasound-stimulated microbubble and radiation therapy, we used high-frequency 3-D power Doppler ultrasound. Ultrasound Doppler imaging techniques rely on moving red blood cells to yield flow velocity estimates and tumor perfusion. These techniques are, however, limited by poor resolution and are susceptible to a number of artifacts including aliasing artifacts. Power Doppler ultrasound is an effective and inexpensive imaging modality for quantifying tumor vasculature and is capable of overcoming some of the main limitations encountered in conventional Doppler ultrasound imaging (Foster et al. 2000; Gee et al. 2001; Goertz et al. 2002). It works by measuring the total integrated power of all Doppler-shifted frequencies, rather than by obtaining an average estimate of Doppler-shifted frequencies (such as in color Doppler). Because of this, power Doppler is minimally angle dependent and more sensitive to low-velocity blood flow. At high frequencies, power Doppler is even more sensitive to slow blood flow in tumor microvasculature, permitting the detection of vessels down to approximately 50–150 μm, and has greater resolution than conventional clinical ultrasound frequency ranges (Goertz et al. 2002). This makes it a suitable modality with which to assess tumor vascular responses to vascular targeting therapies in studies involving a large number of therapeutic conditions or permutations of combined therapies. Power Doppler has been used to quantify vasculature changes after treatment of pre-clinical tumors, as evaluated extensively in the literature (Donnelly et al. 2001; El Kaffas et al. 2013; Gee et al. 2001; Kim et al. 2006; Palmowski et al. 2008; Su et al. 2006).

In this study, we used high-frequency 3-D power Doppler ultrasound, histologic assays of cell death and tumor growth delay measurements to demonstrate that ultrasound-activated microbubbles can enhance the effects of radiation in breast cancer cells *in vivo*. We determined the effects on blood flow and blood vessel-lining endothelial cells of combined ultrasound-activated microbubbles and radiation therapy. We measured the immediate and longitudinal *in vivo* vascular responses of these therapies. The data indicates that particularly when combined with 2 Gy doses of radiation, ultrasound treatment has a potentiating effect.

METHODS

All experiments on animals described in this article were conducted in compliance with internationally recognized guidelines specified in protocols approved by the Sunnybrook Health Science Centre Institutional Animal Care and Use Committee. Human MDA-MB-231 breast cancer xenografts were grown in the left upper hind leg of Swiss nude mice. Tumors were grown to approximately 8 mm in diameter before treatment, which took around 3–4 wk. During treatment, mice were anesthetized with an intraperitoneal injection of ketamine 100 mg/kg, xylazine 5 mg/kg and acepromazine 1 mg/kg in 0.9% sodium chloride (saline) titrated at 0.02 mL intervals to a maximum dose of 0.1 mL. A total of 56 animals were used for this study.

Definity microbubbles (perfluoropropane gas/liposome shell, Lantheus Medical Imaging, North Billerica, MA, USA) were administered through a tail vein catheter at different volume concentrations (0, 0.5% and 3% v/v). Animals were then immersed in a water bath at 37°C for ultrasound exposure. The ultrasound therapy system comprised a micro-positioning system, waveform generator (AWG520, Tektronix, Beaverton, OR, USA), power amplifier with pulser/receiver (RPR4000, Ritec, Rochester, NY, USA) and a digital acquisition system (CC103, Agilent, Monroe, NY, USA). Animals were exposed within the half-maximum peak of the acoustic signal (-6 dB beam width = 31 mm, depth of field >2 cm) 16 cycle tone burst at 500 kHz center frequency using a 2.85 cm unfocused planar ultrasound transducer (ILO509 HP, Valpey Fisher, Hopkinton, MA, USA) and at 3 kHz pulse repetition frequency for 50 ms at a time with a peak negative pressure set to 570 kPa, corresponding to a mechanical index (MI) of 0.8. An intermittent 1950 ms period between sonifications was employed to minimize biological heating in the tissue during ultrasound exposures. The total insonification time was 750 ms over 5 min, for an overall duty cycle of 0.25%.

Immediately after ultrasound exposure, mice were shielded using a 3-mm lead shield, and only the tumor was exposed to ionizing radiation (Faxitron Cabinet X-ray, Faxitron X-Ray, Lincolnshire, IL, USA) at doses of 0, 2 or 8 Gy in single fractions. X-rays were administered at an energy of 160 kVp, a source-skin distance of 35 cm and a dose rate of 200 cGy/min. Instrumentation was

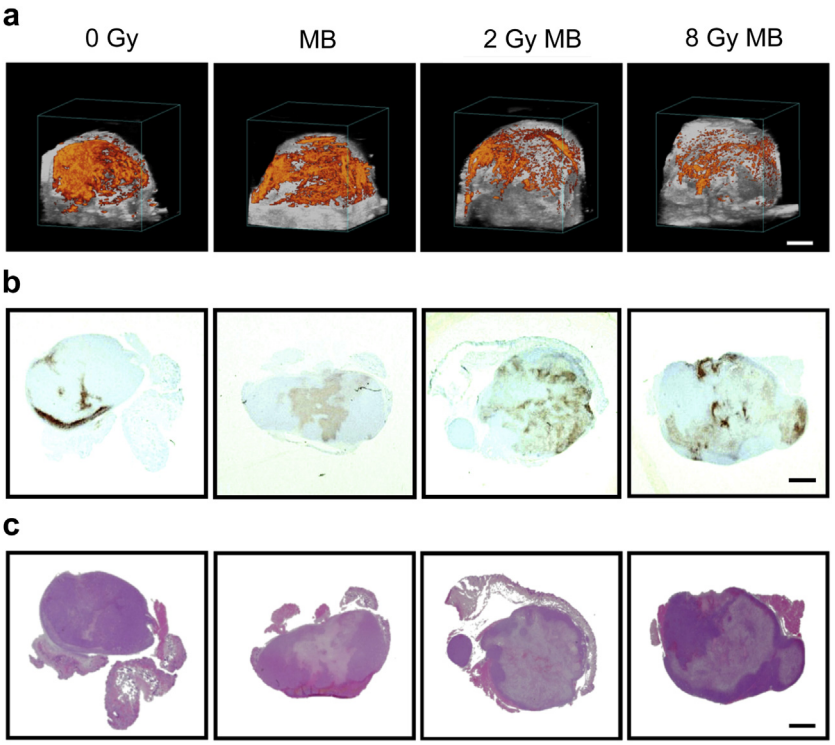

Fig. 1. (a) Representative 3-D power Doppler images of tumors 24 h after treatment. Tumors treated with combined ultrasound-activated microbubble (MB) and radiation treatments and higher doses of radiation had significantly less vasculature. Power Doppler images were analyzed by determining the vascular index (VI), which is the ratio of the total number of color voxels (flow signal) to the total number of voxels in the region of interest. Scale bar = 5 mm. (b) Tumor samples were stained by *in situ* end labeling (ISEL) to identify regions of apoptotic DNA fragmentation, seen as brown patches. There is significantly more apoptosis in treated samples than in the control. Without microbubbles, the proportions of apoptosis were 5 ± 4%, 15 ± 2% and 14 ± 3% for the control (0 Gy), 2 Gy and 8 Gy treatments, respectively. With microbubbles, these increased to 40 ± 15%, 60 ± 15% and 57 ± 10%, respectively. Scale bar = 2 mm. (c) Hematoxylin and eosin staining of tumor samples revealed increased cell death with higher doses of radiation combined with ultrasound-activated microbubbles. These results support power Doppler data linking cell death with vasculature damage. Scale bar = 2 mm.

calibrated for radiation dose delivery and validated using X-ray film and solid-state dosimetry.

Mice were imaged before and after treatment with a VEVO-770 (Visualsonics, Toronto, ON, Canada) in power Doppler mode and a VEVO RMV transducer with a central frequency of 20 MHz. Power Doppler imaging settings included a wall filter of 2.5 mm/s, a scan speed of 2.0 mm/s, a gain of 20 dB and a step size of 0.2 mm. During imaging, mice remained anesthetized and were also restrained using a custom sleeve to prevent motion artifacts. Mice were imaged before and 3 hours (h), 24 h and 7 days (d) after treatment. Power Doppler data were analyzed to quantify relative changes in vasculature.

Power Doppler data were analyzed using custom-written MATLAB (Mathworks, Natick, MA, USA) software. Regions of interest (ROIs) were selected for each frame of the 3-D tumor volume to include tumor tissue only, and every frame in which the tumor was clearly defined was used in the analysis. The vascularization index (VI) was defined as the ratio of the volume of all colored pixels to the volume of all selected regions of interest. The VI was computed by dividing the number of colored voxels by the total number of voxels for all selected ROIs. The VI was used to represent the amount of vasculature in the tumor. In this study, we report on the relative VI as it changes over 3 h, 24 h and 7 d. The relative VI was defined as $(VI_{\text{treatment time point}}/VI_{\text{pre-treatment}}) \times 100$. Statistical analysis with the Mann-Whitney test (two-tailed, assuming unequal variances) were performed at 24-h time points using Prism (GraphPad Software, La Jolla, CA, USA). Each treatment condition was compared with the control condition. The control condition was comprised of completely untreated tumors.

At least three mice from each treatment condition were used to conduct a tumor growth delay study. The length, width and height of each tumor were measured before treatment (day 0) and every third day over a 24 d period. Tumor volumes were approximated

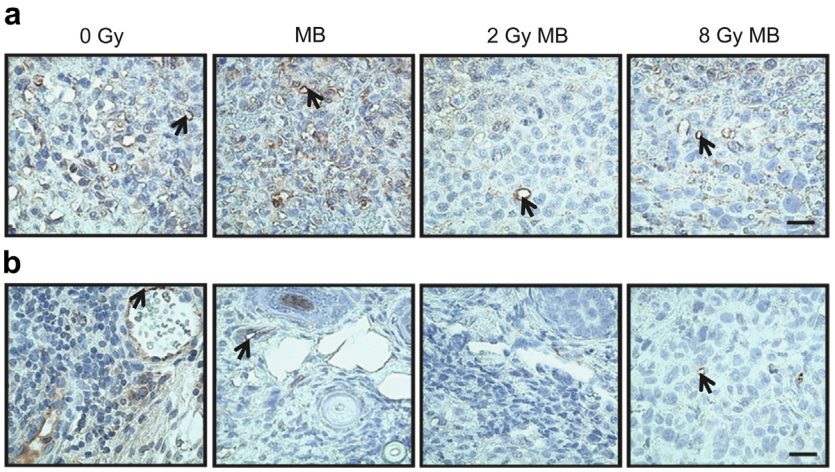

Fig. 2. Anti-vascular endothelial growth factor (VEGF) antibodies (a) and anti-CD31 antibodies (b) were used to stain for tumor endothelium. Positive staining (red-brown) indicates presence of endothelial cells, which are also indicated by the *arrows*. Scale bar = 25 μm. Results indicated less endothelium for combined treatments with higher doses of radiation. Without microbubbles, the quantified CD31 staining was 1 ± 3%, 0.77 ± 0.04% and 0.5 ± 0.2% for the control (0 Gy), 2 Gy and 8 Gy treatments respectively. With microbubbles (MB), the proportions of CD31 staining were 0.6 ± 0.1%, 0.5 ± 0.1% and 0.2 ± 0.1%, respectively.

as volume = (length × width × height × π)/6. Tumor growth delay data were normalized to the initial tumor volume, yielding a relative tumor volume.

Histology was conducted on tumor samples excised immediately after animal sacrifice, 24 h post-treatment, as a method of supporting conclusions made by power Doppler data. Tumor samples were fixed overnight at room temperature in 1% paraformaldehyde, embedded in paraffin blocks and sectioned into 5-μm slices for histology. Standard hematoxylin and eosin (H&E) and *in situ* end labeling (ISEL) staining were conducted (Pathology Research Program, University Health Network, Toronto, ON, Canada). ISEL staining was used to identify inter-nucleosomal DNA fragmentation as evidence of apoptosis. Images were digitized, and the amount of apoptotic cell death was quantified using ImageJ (National Institutes of Health, Bethesda, MD, USA).

Immunohistochemistry was performed using the Histostain-Plus Kit (Invitrogen, Carlsbad, CA, USA), according to the manufacturer's instructions and as previously described (Al-Mahrouki et al. 2012). Tumor vasculature was stained with anti-vascular endothelial growth factor (VEGF) antibodies and anti-CD31 antibodies. Both CD31 and VEGF antibodies were obtained from Abcam (Cambridge, MA, USA). Anti-CD31 targets platelet endothelial cell adhesion molecules (PECAM-1) expressed on endothelial cells. The percentage of CD31-stained vessels was determined by manually counting the number of intact and disrupted vessels using Leica IM1000 software with a Leica DM LB light microscope. Percentage of CD31-stained vessels is defined as the ratio of the number of intact luminal vessels to the total number of vessels measured within a region of interest. The entire cross-sectional area of one tumor slice in each animal tumor was quantified.

RESULTS

Representative 3-D power Doppler images taken 24 h after ultrasound and radiation treatment are provided in Figure 1a. Power Doppler images of treated tumors revealed a decrease in blood flow signal compared with controls and even greater decreases in signal with combined treatments and larger doses of radiation. Corresponding low-magnification immunohistochemistry (Figs. 1b, c and 2) revealed both increased cell death and increased endothelial cell kill with combined treatments and the higher radiation dose, supporting a link between damage to the vasculature and tumor cell death.

Staining with ISEL was used to quantify DNA fragmentation as evidence of apoptotic cell death in tumor samples 24 h post-treatment (Fig. 3a). DNA fragmentation is visualized as patches of brown, the number and area of which are increased in treated samples compared to controls (Fig. 1b). Quantitatively (Fig. 3a), the proportions of cell death after the control (0 Gy), 2 Gy and 8 Gy treatments were 5 ± 4%, 15 ± 2% and 14 ± 3%, respectively. With ultrasound-activated microbubbles, these proportions increased to 40 ± 15%, 60 ± 15% and 57 ± 10%, respectively. H&E staining was used to assess the proportion of total cell death in the tumor samples 24 h post-treatment (Fig. 1c). Areas of cell death are identified as whitened or blanched areas, which increased with different treatments. A central region of cell death was also observed in treated tumors compared with the

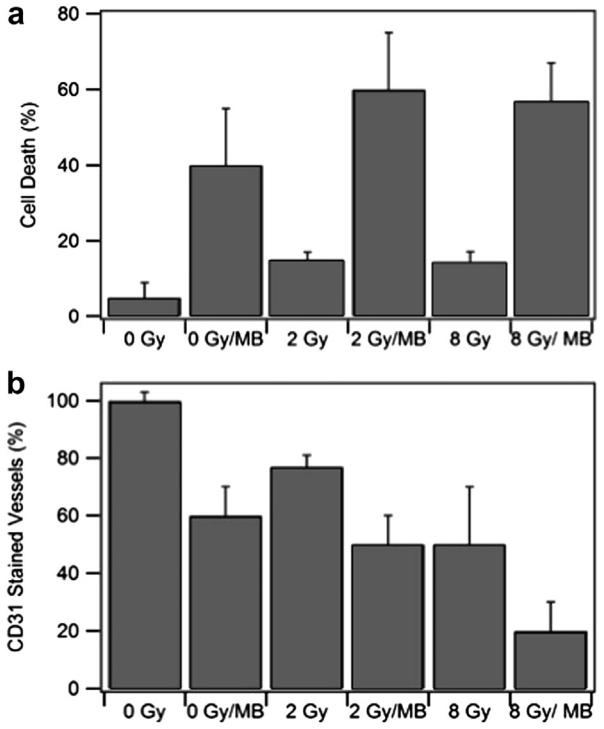

Fig. 3. Quantification of cell death and vasculature from tumor cross sections subjected to *in situ* end labeling (ISEL) (a) and CD31 staining (b). In (a), we find a slight increase in cell death for tumors treated with radiation alone. We also find greater cell death for all conditions in which microbubbles (MB) were used, whether alone or in combination with radiation. In (b), we find a ∼50% decrease in CD31 staining for 8 Gy alone. Microbubbles alone also caused a ∼30–40% decrease in CD31 staining. However, combining both microbubbles and radiation yielded the greatest decrease in CD31 staining. This suggests that microbubbles radiosensitized endothelial cells, leading to acute endothelial cell death.

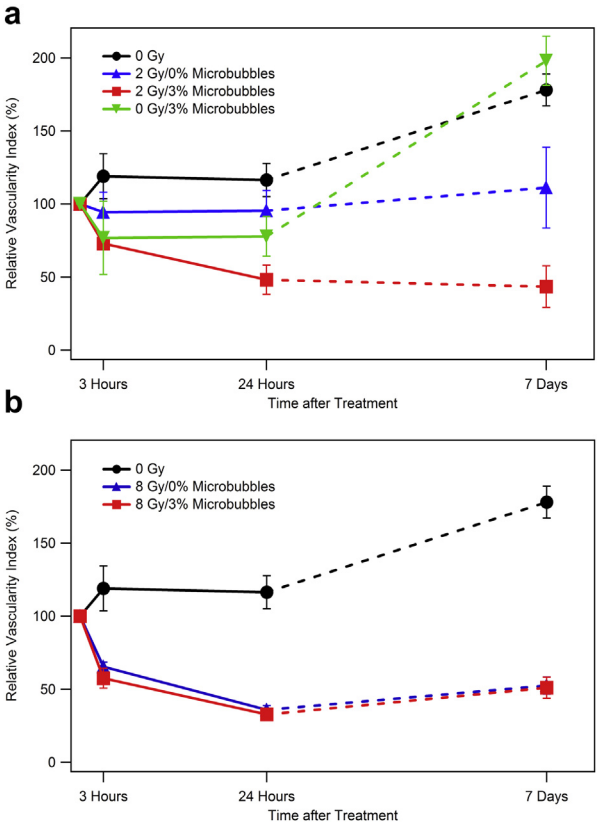

Fig. 4. Vascular index (VI) quantified from volumetric power Doppler images. (a) VIs of tumors treated with 2 Gy radiation and 3% microbubbles (red) decreased to 73 ± 2% at 3 h, 48 ± 10% at 24 h and 43 ± 14% at 7 d. VIs of tumors treated with 2 Gy radiation alone (blue) remained relatively unchanged at 94 ± 14% at 3 h, 95 ± 14% at 24 h and 111 ± 28% at 7 d. These results indicate a significant enhancement in tumor vasculature kill caused by ultrasound-activated microbubbles. Error bars represent standard errors. VIs of tumors treated with 0 Gy radiation and 3% microbubbles (red) initially decreased to 77 ± 25% at 3 h and 78 ± 14% at 24 h, before increasing to 198 ± 17% at 7 d. VIs of untreated tumors increased to 119 ± 15% at 3 h and 116 ± 11% at 24 h, before increasing to 178 ± 11% at 7 d. These results indicate that microbubbles alone are insufficient to cause tumor vasculature damage over 7 d. Because tumors treated with 2 Gy radiation alone did not experience significant changes in vasculature, we propose that ultrasound-activated microbubbles enhance 2 Gy radiation treatments through a synergistic mechanism. (b) VIs of tumors treated with 8 Gy radiation and 3% microbubbles (red) decreased to 58 ± 7% at 3 h, 33 ± 1% at 24 h and 51 ± 7% at 7 d. VIs of tumors treated with 8 Gy radiation alone (blue) had similar changes, decreasing to 65 ± 3% at 3 h, 36 ± 3% at 24 h and 53 ± 6% at 7 d. These results suggest that ultrasound-activated microbubbles are not effective at enhancing the effects of 8 Gy radiation.

control. Tumor specimens were subjected to VEGF and CD31 staining 24 h post-treatment to assess the effect of treatment on endothelial cells (Fig. 2a, b). Both staining methods revealed evidence of a decrease in the percentage vasculature with different treatments, identified as decreased brown-red staining of discernable intact vessels. For the control (0 Gy), 2 Gy and 8 Gy treatments, the quantified proportions of CD31-stained vessels were 100 ± 3%, 77 ± 4% and 50 ± 20%. In the presence of ultrasound-activated microbubbles, these proportions were 60 ± 10%, 50 ± 10% and 20 ± 10% (Fig. 3b).

Longitudinal studies using power Doppler imaging were undertaken to non-invasively assess treatment effects on blood flow. The power Doppler-based VI, a measure of the percentage of active vasculature in a tumor, was computed relative to a baseline determined before treatment. Data are expressed as the mean vascular index ± standard error of the mean in Figure 4. Quantified VIs after all 8 Gy treatments and the combined 2 Gy microbubble treatments were found to significantly differ from those of controls ($p < 0.05$) at 24 h. However, VIs after treatment with 2 Gy radiation alone ($p = 0.11$) or microbubbles alone ($p = 0.14$) did not statistically significantly differ from those of controls.

Tumors treated with 2 Gy radiation experienced greater vascular destruction with combined treatments than with radiation only (Fig. 4a). The VIs of tumors treated with 2 Gy radiation and ultrasound-activated microbubbles decreased from baseline to 73 ± 2% at 3 h, 48 ± 10% at 24 h and 43 ± 14% at 7 d. In comparison, tumors treated with 2 Gy radiation alone underwent very little initial change in blood flow and an eventual increase in power Doppler signal 7 d after treatment (VIs for 2 Gy condition: 94 ± 14% at 3 h, 95 ± 14% at 24 h and 111 ± 28% at 7 d). The added presence of ultrasound-activated microbubbles elicited a nearly twofold decrease in vascular flow compared with radiation alone at 24 h, supporting the observation that microbubbles can enhance the effect of radiation on blood vessels.

Treatment with ultrasound-activated microbubbles alone was not sufficient to disrupt tumor vasculature significantly when compared to control tumors. After treatment of tumors with 0 Gy and ultrasound-activated microbubbles, the VI decreased initially to 77 ± 25% at 3 h and 78 ± 14% at 24 h, before increasing significantly to 198 ± 17% at 7 d. This appeared to be re-perfusion of the tumor. In comparison, VIs of completely untreated tumors were 119 ± 15% at 3 h, 116 ± 11% at 24 h and 178 ± 11% at 7 d. Tumors treated with 8 Gy radiation alone experienced significantly more vascular damage than tumors treated with 2 Gy radiation (Fig. 4b); VIs decreased to 65 ± 3% at 3 h, 36 ± 3% at 24 h and 53 ± 6% at 7 d. On the other hand, combined treatments with 8 Gy radiation and ultrasound-activated microbubbles did not significantly reduce blood flow (VI = 58 ± 7% at 3 h, 33 ± 1% at 24 h and 51 ± 7% at 7 d).

We examined the effects of single-fraction (0, 2 and 8 Gy) radiation treatments with and without ultrasound-activated microbubbles on tumor growth delay over a 24 day period after treatment (Fig. 5). The mean relative tumor volumes ± standard errors of at least three mice for each treatment are plotted. Although statistically significant effects are observed in quantified power Doppler and histology, this does not currently translate to a significant growth delay; a weak trend towards a slower growth is observed, consistent with vascular damage. Tumors treated with 8 Gy and ultrasound-activated microbubbles had the longest growth delay and smallest increase in volume, whereas tumors treated with 0 Gy and ultrasound-activated microbubbles had the largest increase in volume in comparison to other non-control conditions.

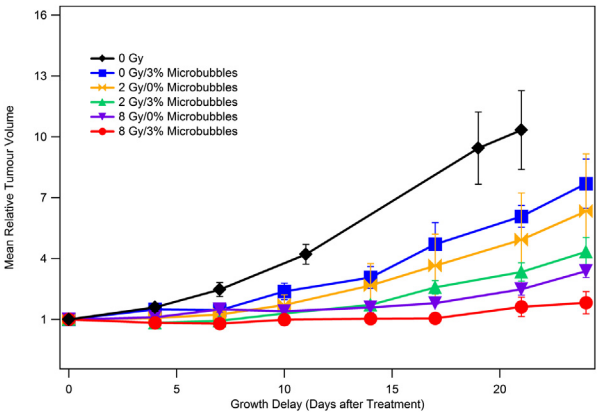

Fig. 5. Tumor growth is in qualitative agreement with power Doppler results. The untreated tumors had the largest increases in tumor volume over the 24 day period, followed by tumors treated with 0 Gy and 3% microbubbles. The smallest increase in tumor volume was for tumors treated with 8 Gy and 3% microbubbles. At least three mice were used for each curve. Error bars represent standard errors.

DISCUSSION

Ultrasound-activated microbubbles substantially enhanced the effects of 2 Gy radiation at 3 h, 24 h and 7 d, eliciting significant changes in blood flow as assessed using 3-D high-frequency power Doppler ultrasound. These results were interpreted as sustained vascular damage to tumor vasculature. As power Doppler is predominantly sensitive to flow in larger vessels (>150–50 μm) of the tumor, which feed the smaller capillaries of the microcirculation, a rapid decrease in the VI likely resulted in tumor vascular shutdown and tumor necrosis. In addition, vascular damage in terms of a decreased vascular index was detected 24 h after treatment using immunohistochemistry, further confirming our results using power Doppler ultrasound imaging.

As expected, 2 Gy doses of radiation alone were not sufficient to suppress tumour vasculature blood flow in a consistent manner (Fig. 4a). Tumors treated with microbubbles alone experienced a decrease in detected blood flow followed by a sharp increase in vasculature by 7 d (Fig. 4b). Other studies have reported that ultrasound-activated microbubbles alone can be used to therapeutically induce arteriogenesis, angiogenesis and neovascularization in mouse skeletal muscle (Chappell and Price 2006; Chappell et al. 2005; Song et al. 2002).

We propose that the combination of ultrasound-activated microbubbles and 2 Gy radiation enhances the effects of radiation on the microvasculature through a synergistic mechanism. The effect detected seems to be more than additive, especially 7 d after treatment, at which point a rebound was detected in tumors treated with only ultrasound-activated microbubbles.

Tumors treated with 8 Gy radiation alone had significantly more vascular damage than those treated with 2 Gy radiation alone. These results support previous research suggesting that high doses of radiation can

directly affect tumor vasculature (Garcia-Barros et al. 2003; Paris et al. 2001), in contrast to low doses of radiation, typically delivered in 2 Gy fractions, which indirectly affect vasculature primarily through hypoxia, reperfusion and formation of reactive oxygen species (Fuks and Kolesnick 2005). The vasculature of tumors treated with 8 Gy radiation was not significantly affected by the presence of ultrasound-activated microbubbles. This suggests that ultrasound-activated microbubbles may be more suitable for use in conjunction with lower doses of radiation.

A number of studies have reported the use of anti-angiogenic agents or vascular disrupting agents (VDAs) as tumor radiosensitizers (El Kaffas et al. 2013; Small 2008; Wachsberger et al. 2003). However, the exact mechanisms underlying the interaction of these agents with radiotherapy remain unknown (Tozer et al. 2005). Ultrasound-activated microbubbles are a novel biophysical alternative to traditional chemical VDAs for enhancing the effects of radiation. There is evidence that microbubbles act by mechanically damaging cell membranes (Kudo et al. 2002; Truong An et al. 2008). However, ongoing research in our laboratory has suggested activation of the ceramide pathway as a biological mechanism of interaction. Ceramide is a second messenger molecule generated by the enzyme acid sphingomyelinase at the cell membrane, which can be activated in response to cellular stress (Hannun and Obeid 2002). Ceramide was observed to increase in cells treated with ultrasound-activated microbubbles and is potentially an important contributor to endothelial apoptosis and vascular disruption observed *in vivo* (Czarnota et al. 2012).

A major advantage of this method is that ultrasound is focused only on the tumor to cause microbubble perturbations. In this way, only the tumor is radiosensitized, reducing effects on surrounding normal tissue. In addition, the low-intensity pulsed ultrasound used in this study is non-invasive and causes no significant morbidity in normal tissue. The ultrasound parameters were in the diagnostic exposure range, and no heating effects were observed. This contrasts starkly with other anti-tumor treatments involving ultrasound, including high-intensity focused ultrasound (HIFU), which ablates local tissue with the high temperatures generated by the focused ultrasound beam (Haar and Coussios 2007).

In this work, we determined that the use of ultrasound-activated microbubbles is a considerably promising technique to enhance the therapeutic efficacy of radiation treatment in cancer. A prime observation appears to be its effects on blood vessels, which are observed as changes in blood flow. Future work includes studies in various other animal models and cancer cell lines to examine the time kinetics of the observed synergistic effect and the dosing required for an optimal radiation and microbubble combination.

Acknowledgments—This work was supported by the Canadian Breast Cancer Foundation and the Terry Fox Foundation through the program project grant Ultrasound for Cancer Therapy. Aspects of the work were also supported by a Cancer Care Ontario (CCO) research grant in experimental therapeutics and imaging. Finally, the authors thank Dr. Kerbel for his generous donation of MDA-MB-231 cells. Dr. Gregory Czarnota is supported by a CCO Research Chair in Experimental Therapeutics and Imaging.

REFERENCES

Al-Mahrouki AA, Karshafian R, Giles A, Czarnota GJ. Bioeffects of ultrasound-stimulated microbubbles on endothelial cells: Gene expression changes associated with radiation enhancement in vitro. Ultrasound Med Biol 2012;38:1958–1969.

Chappell JC, Klibanov AL, Price RJ. Ultrasound-microbubble-induced neovascularization in mouse skeletal muscle. Ultrasound Med Biol 2005;31:1411–1422.

Chappell JC, Price RJ. Targeted therapeutic applications of acoustically active microspheres in the microcirculation. Microcirculation 2006; 13:57–70.

Czarnota GJ, Karshafian R, Burns PN, Wong S, Al Mahrouki A, Lee J, Caissie A, Tran WT, Kim C, Furukawa M, Wong E, Giles A. Tumour radiation response enhancement by acoustical stimulation of the vasculature. Proc Natl Acad Sci USA 2012;109:E2033–EE2041.

Donnelly EF, Geng L, Wojcicki WE, Fleischer AC, Hallahan DE. Quantified power Doppler US of tumor blood flow correlates with microscopic quantification of tumor blood vessels. Radiology 2001;219: 166–170.

El Kaffas A, Giles A, Czarnota GJ. Dose-dependent response of tumor vasculature to radiation therapy in combination with sunitinib depicted by three-dimensional high-frequency. Angiogenesis 2013; 16:443–454.

El Kaffas A, Tran W, Czarnota GJ. Vascular strategies for enhancing tumour response to radiation therapy. Technol Cancer Res Treat 2012;11:409–527.

Folkman J, Camphausen K. Cancer: What does radiotherapy do to endothelial cells? Science 2001;293:227–228.

Foster FS, Burns PN, Simpson DH, Wilson SR, Christopher DA, Goertz DE. Ultrasound for the visualization and quantification of tumor microcirculation. Cancer Metast Rev 2000;19:131–138.

Fuks Z, Kolesnick R. Engaging the vascular component of the tumor response. Cancer Cell 2005;8:89–91.

Garcia-Barros M, Paris F, Cordon-Cardo C, Lyden D, Rafii S, Haimovitz-Friedman A, Fuks Z, Kolesnick R. Tumor response to radiotherapy regulated by endothelial cell apoptosis. Science 2003;300:1155–1159.

Gee MS, Saunders HM, Lee JC, Sanzo JF, Jenkins WT, Evans SM, Trinchieri G, Sehgal CM, Feldman MD, Lee WM. Doppler ultrasound imaging detects changes in tumor perfusion during antivascular therapy associated with vascular anatomic alterations. Cancer Res 2001;61:2974–2982.

Goertz DE, Yu JL, Kerbel RS, Burns PN, Foster FS. High-frequency Doppler ultrasound monitors the effects of antivascular therapy on tumor blood flow. Cancer Res 2002;62:6371–6375.

Haar GT, Coussios C. High intensity focused ultrasound: Physical principles and devices. Int J Hyperthermia 2007;23:89–104.

Hannun YA, Obeid LM. The ceramide-centric universe of lipid-mediated cell regulation: Stress encounters of the lipid kind. J Biol Chem 2002;277:25847–25850.

Hwang JH, Brayman AA, Reidy MA, Matula TJ, Kimmey MB, Crum LA. Vascular effects induced by combined 1-MHz ultrasound and microbubble contrast agent treatments in vivo. Ultrasound Med Biol 2005;31:553–564.

Kim DWN, Huamani J, Niermann KJ, Lee H, Geng L, Leavitt LL, Baheza RA, Jones CC, Tumkur S, Yankeelov TE, Fleischer AC, Hallahan DE. Noninvasive assessment of tumor vasculature response to radiation-mediated, vasculature-targeted therapy using

quantified power Doppler sonography: Implications for improvement of therapy schedules. J Ultrasound Med 2006;25:1507–1517.
Kudo N, Miyaoka T, Okada K, Yamamoto K, Niwa K. Study on mechanism of cell damage caused by microbubbles exposed to ultrasound. IEEE Ultrasonics Symposium 2002;1383–1386.
Lehnert S. Biomolecular action of ionizing radiation. New York: Taylor & Francis; 2007.
Palmowski M, Huppert J, Hauff P, Reinhardt M, Schreiner K, Socher MA, Hallscheidt P, Kauffmann GW, Semmler W, Kiessling F. Vessel fractions in tumor xenografts depicted by flow- or contrast-sensitive three-dimensional high-frequency Doppler ultrasound respond differently to antiangiogenic treatment. Cancer Res 2008;68:7042–7049.
Paris F, Fuks Z, Kang A, Capodieci P, Juan G, Ehleiter D, Haimovitz-Friedman A, Cordon-Cardo C, Kolesnick R. Endothelial apoptosis as the primary lesion initiating intestinal radiation damage in mice. Science 2001;293:293–297.
Qin SP, Ferrara KW. The natural frequency of nonlinear oscillation of ultrasound contrast agents in microvessels. Ultrasound Med Biol 2007;33:1140–1148.
Small W. Combining targeted biological agents with radiotherapy: Current status and future directions. New York: Demos Medical; 2008.
Song J, Qi M, Kaul S, Price RJ. Stimulation of arteriogenesis in skeletal muscle by microbubble destruction with ultrasound. Circulation 2002;106:1550–1555.
Su JM, Huang YF, Chen HHW, Cheng YM, Chou CY. Three-dimensional power Doppler ultrasound is useful to monitor the response to treatment in a patient with primary papillary serous carcinoma of the peritoneum. Ultrasound Med Biol 2006;32:623–626.
Tozer GM, Kanthou C, Baguley BC. Disrupting tumour blood vessels. Natl Rev Cancer 2005;5:423–435.
Truong An T, Le Guennec JY, Bougnoux P, Tranquart F, Bouakaz A. Characterization of cell membrane response to ultrasound activated microbubbles. IEEE Trans Ultrasonics Ferroelectr Freq Control 2008;55:43–49.
Unger EC, Matsunaga TO, McCreery T, Schumann P, Sweitzer R, Quigley R. Therapeutic applications of microbubbles. Eur J Radiol 2002;42:160–168.
Unger EC, Porter T, Culp W, Labell R, Matsunaga T, Zutshi R. Therapeutic applications of lipid-coated microbubbles. Adv Drug Deliv Rev 2004;56:1291–1314.
Wachsberger P, Burd R, Dicker AP. Tumor response to ionizing radiation combined with antiangiogenesis or vascular targeting agents: Exploring mechanisms of interaction. Clin Cancer Res 2003;9:1957–1971.
Wilson SR, Burns PN. Microbubble contrast for radiological imaging: 2. Applications. Ultrasound Q 2006;22:15–18.
Wu J, Nyborg WL. Ultrasound, cavitation bubbles and their interaction with cells. Adv Drug Deliv Rev 2008;60:1103–1116.